Multipath Wide-Bandwidth CMOS Magnetic Sensors

Junfeng Jiang and Kofi A. A. Makinwa, *Fellow, IEEE*

***Abstract*— This paper proposes a multipath multisensor architecture for CMOS magnetic sensors, which effectively extends their bandwidth without compromising either their offset or resolution. Two designs utilizing the proposed architecture were fabricated in a 0.18-μm standard CMOS process. In the first, the combination of spinning-current Hall sensors and nonspun Hall sensors achieves an offset of 40 μT and a resolution of 272 μT_{rms} in a bandwidth of 400 kHz, which is 40 times more than previous low-offset CMOS Hall sensors. In the second, the combination of spinning-current Hall sensors and pickup coils achieves the same offset, with a resolution of 210 μT_{rms} in a further extended bandwidth of 3 MHz, which is the widest bandwidth ever reported for a CMOS magnetic sensor.**

***Index Terms*— CMOS, Hall sensor, magnetic sensor, multipath, pickup coil, ripple reduction loop (RRL).**

I. Introduction

CURRENT measurements are widely required in many applications, e.g., motor controls, overload detections, and energy monitoring systems. Traditional shunt-based current sensors [1] suffer from poor galvanic isolation. To improve this, magnetic sensors are often used as contactless current sensors, with the added advantage that the current-carrying path does not need to be broken, allowing them to be easily retrofitted to existing systems [2]. Compared with other types of magnetic sensors, such as magnetoresistive [3] sensors and fluxgates [4], [5], Hall sensors have found the widest application, mainly because of their wider dynamic range, compatibility with standard CMOS processes, and hence low fabrication cost.

However, due to their limited sensitivity, the accuracy of state-of-the-art CMOS Hall sensors is severely impacted by their offset, which ranges from a few microteslas [6] to a few milliteslas [7]. Moreover, the achievable current-to-magnetic field sensitivity is limited by packaging constraints on the distance between the sensor and the current-carrying conductor. In [8], a 30-mA detectable current was achieved by a 10-μT offset Hall sensor, with the help of a lead-frame-based current-carrying conductor.

Manuscript received May 5, 2016; revised August 28, 2016; accepted October 13, 2016. Date of publication November 21, 2016; date of current version January 4, 2017. This paper was approved by Guest Editor Roman Genov. This work was supported by Texas Instruments for Chip Fabrication.

J. Jiang is with the Electronic Instrumentation Laboratory, Delft University of Technology, Delft, The Netherlands, and also with Texas Instruments Deutschland GmbH, 85356 Freising, Germany (e-mail: j-jiang@ti.com).

K. A. A. Makinwa is with the Electronic Instrumentation Laboratory, Delft University of Technology, Delft, The Netherlands.

Color versions of one or more of the figures in this paper are available online at http://ieeexplore.ieee.org.

Digital Object Identifier 10.1109/JSSC.2016.2619711

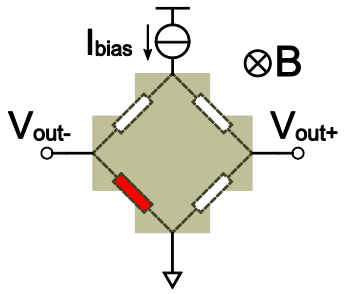

Fig. 1. Model of a CMOS Hall sensor.

In addition to a requirement on accuracy, a bandwidth of a few megahertz [9] [10] is often required in some applications, such as switched-mode power supplies, to capture rapid current transients. This wide bandwidth requirement is even more crucial in overload/short-circuit detection [11], [12], where for safety concerns, detection time in the order of a few microseconds is often required [13]. However, the state-of-the-art CMOS magnetic sensors are typically optimized for either low offset [6], [8], [14] or wide bandwidth [15], but not for both.

In CMOS processes, Hall sensors can be built as four-contact n-well plates and modeled as a Wheatstone bridge, as shown in Fig. 1. When biased at a current level I_{bias}, the Hall plate produces an output voltage V_{out} at the other two terminals in the presence of a magnetic field perpendicular to the plate, which can be expressed as

$$V_{out} = S_{HS} \cdot I_{bias} \cdot B \tag{1}$$

where S_{HS} is the current related sensitivity of the Hall sensor in V/AT. The sensitivities of CMOS Hall sensors depend on several process and layout parameters, with typically reported values ranging from 100 to 400 V/AT [16]–[19]. For a magnetic field of 1 mT, a typical Hall sensor with a biasing current of 1 mA can only produce an output signal of 100–400 μV. At the expense of extra fabrication cost, the limited sensitivity of Hall sensors can be improved by an order of magnitude with the help of flux concentrators, which can be realized by depositing a ferromagnetic layer above the sensor [20], [21]. However, spread in concentrator geometry results in extra sensitivity spread [22].

Despite their low fabrication cost and good linearity, Hall sensors exhibit raw offsets of ~10–50 mT, which are often orders of magnitude larger than the signals of interest. This is caused by n-well inhomogeneity, which can be modeled

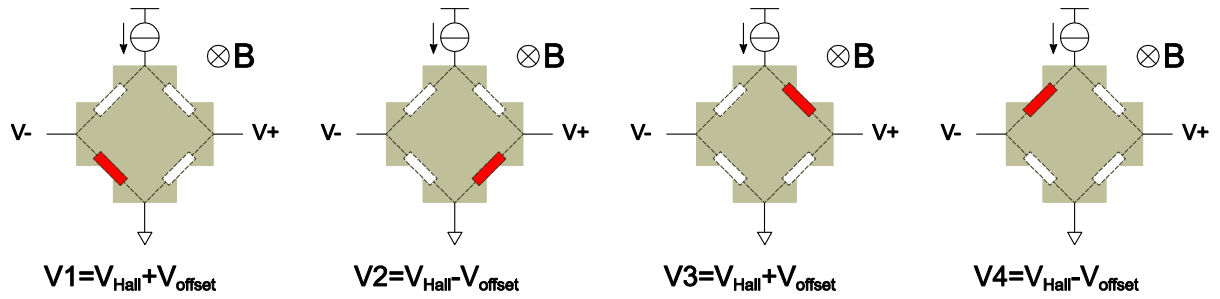

Fig. 2. Operation of the spinning current technique.

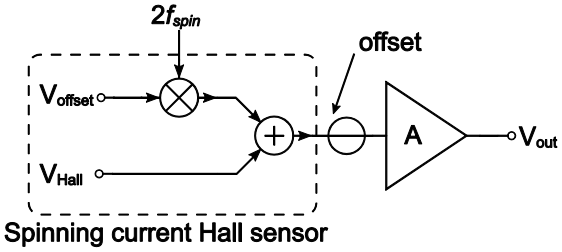

Fig. 3. Extra offset caused by the readout circuitry.

by resistance mismatch in the arms of the corresponding Wheatstone bridge. Fortunately, this offset can be significantly reduced by the well-known spinning current technique, in which the biasing and readout terminals are periodically rotated [23], as shown in Fig. 2. This operation swaps the relative polarities of the sensor's offset V_{offset} and the magnetic signal V_{Hall}, thus modulating V_{offset} to twice the spinning frequency $2f_{\text{spin}}$ and keeping V_{Hall} unaffected. However, due to the necessary amplification of the microvolt level output signal V_{Hall}, low-offset amplifiers are still required to prevent excessive offset, as shown in Fig. 3. To relax this requirement, the spinning current technique can be modified, such that the magnetic signal, instead of the offset, is modulated to $2f_{\text{spin}}$ [14], as shown in Fig. 4. A demodulator, as shown in Fig. 5, can be used to reconstruct the magnetic signal, and simultaneously modulate both the Hall sensor and readout offsets to $2f_{\text{spin}}$. The up-modulated offsets then appear as ac ripple at the amplifier's output. With this approach, CMOS Hall sensors with 10-μT offset can be achieved [8]. This can be further lowered to 4 μT by the use of eight-phase spinning on octagonal Hall sensors [6].

In practice, the amplitude of the spinning ripple is quite large compared with the magnetic signal, and so ripple reduction techniques are necessary. Conventionally, low-pass filters (LPFs) are used, which unfortunately also suppress high-frequency (HF) magnetic signals. In addition to this bandwidth reduction, digital LPFs sample the outputs and therefore suffer from aliasing; while analog LPFs require large time constants to achieve sufficient ripple suppression and therefore occupy considerable area. Although these constraints can be eased by increasing f_{spin}, this is at the expense of an increase in residual offset [15] due to the periodic switching transients and charge injection associated with the spinning current technique. For all the above-mentioned reasons, traditional CMOS Hall sensor designs have to deal with a tradeoff between bandwidth and offset. The bandwidth of low-offset CMOS Hall sensors is thus typically less than 100 kHz [15], despite the fact that the bandwidth of the Hall Effect extends to a few gigahertz [24].

A ripple reduction loop (RRL) [25] can effectively suppress two-phase spinning ripple without the use of LPFs [26]. However, due to the anisotropy of the n-well's resistance, a single RRL cannot fully suppress four-phase spinning ripple [8], as the sensor's offset will change during the various spinning phases. However, any four-phase signal can be fundamentally decomposed into three ripple components and one signal component (the magnetic signal in this case), as shown in Fig. 6. Based on this insight, it has been shown that the ripple of a four-phase spinning current Hall sensor can be significantly reduced by the use of three (off-chip) RRLs [27]. The sensor's useful bandwidth could thus be extended above 100 kHz even with much lower spinning frequencies, e.g., 1 kHz, needed to minimize offset. However, as any signal at the ripple frequencies will be mistaken for ripple, this approach creates notches at f_{spin}, $2f_{\text{spin}}$, and their even-order harmonics, which may cause slow settling issues.

This paper proposes a multipath architecture that combines a wide bandwidth sensor in an HF path with a spinning current Hall sensor (with RRLs) in its low frequency (LF) path. The output of the wide bandwidth sensor will then "fill" up the RRL notches to ensure a flat transfer function. For example, when the wide bandwidth sensor is an ac coupled nonspun Hall sensor [28], the bandwidth of the overall system could be extended to 400 kHz. As the ac coupled nonspun Hall sensor does not introduce extra offset, the system achieves an offset of 40 μT, which is determined by the spinning Hall sensor in the LF path. By replacing the nonspun Hall sensor by a pickup coil in the HF path [29], system bandwidth could be extended, by another order of magnitude, to 3 MHz. Thanks to the differential characteristic of the pickup coils, the hybrid combination of spinning Hall sensors and pickup coils achieves better resolution (210 μT_{rms}) than that of the combination of Hall sensors (272 μT_{rms}), but without consuming more power. These two examples show that the use of a multipath architecture effectively breaks the bandwidth-resolution and bandwidth-offset tradeoffs, and thus enables the realization of wide bandwidth CMOS magnetic sensors.

The rest of this paper is organized as follows. Section II introduces the multipath CMOS magnetic sensor by combining spinning current Hall sensors and nonspun Hall sensors; the combination of spinning current Hall sensors and pickup

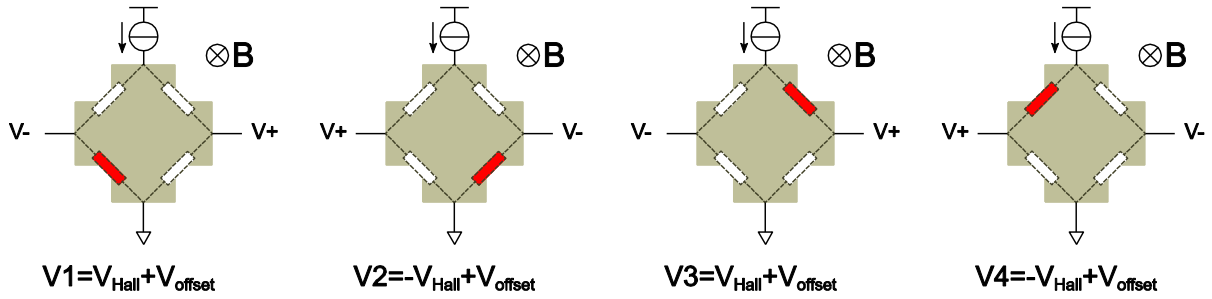

Fig. 4. Slightly modified spinning current algorithm which modulates the magnetic signal to $2f_{\text{spin}}$.

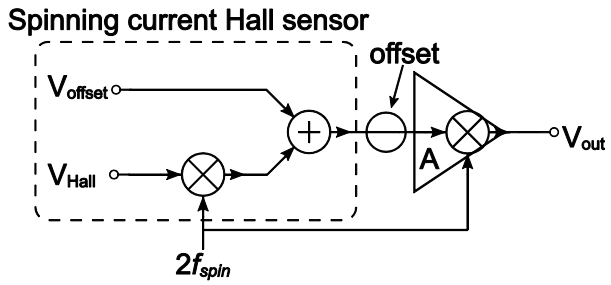

Fig. 5. Demodulator to readout the modified spinning current Hall sensor, where the offsets of the readout and the Hall sensor are merged.

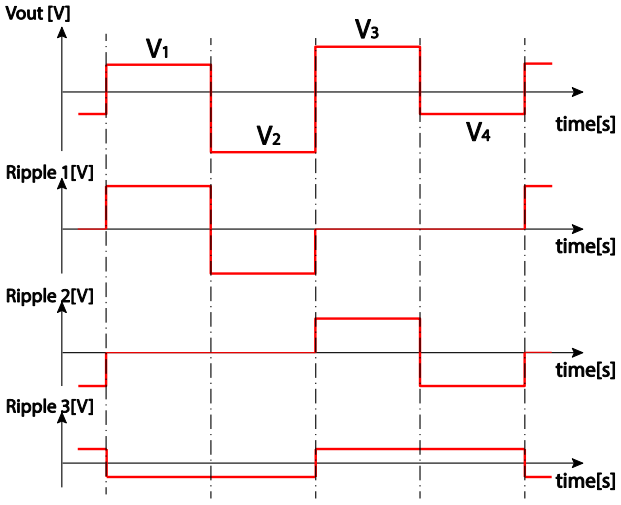

Fig. 6. Four-phase spinning ripple can be decomposed into three orthogonal ripple components.

coils is discussed in Section III; after the discussion of the experiment results in Section IV, the conclusions are drawn in Section V.

II. Multipath Hall Sensor System

A. System Architecture

The proposed system consists of an LF path with a spun Hall sensor and an HF path with a nonspun Hall sensor, as shown in Fig. 7. Both paths use identical Hall sensors and signal paths consisting of two amplifiers: a capacitively coupled amplifier with a gain of 100, and an inverting amplifier with a gain of 20. Both amplifiers have the same bandwidth

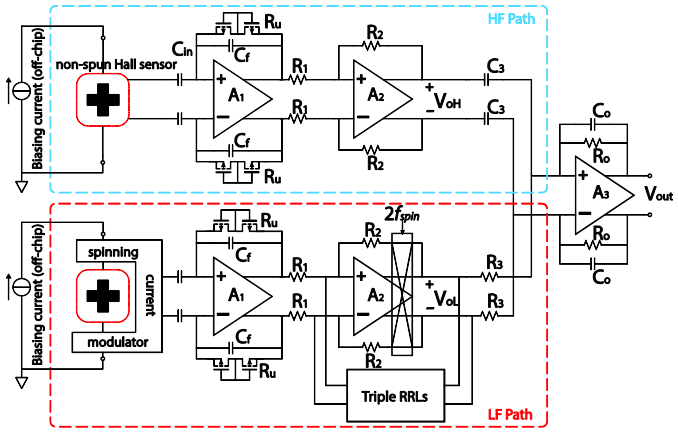

Fig. 7. System diagram of combining a spinning current Hall sensor and a nonspun Hall sensor.

of 400 kHz, so that the overall frequency response will be flat. An output stage with a gain of 2 smoothly combines both paths' outputs by high-pass filtering the output of the HF path and low-pass filtering the output of the LF path, as shown in Fig. 8. The spinning ripple in the LF path is suppressed by the integrated triple RRLs, which inject compensation currents at the virtual ground of A_2. This arrangement greatly relaxes the specification of the triple RRLs due to the large gain of the preceding stage. Any residual ripple will be further suppressed by the first-order low-pass filtering action of the output stage. In this design, the crossover frequency $f_{\text{cross}} = 2$ kHz, and is set by the time constant of R_0C_0 in the feedback of the output stage. This f_{cross} is a compromise between the area and the need to ensure that the notches will be sufficiently filled by the HF path, i.e., $f_{\text{cross}} \ll f_{\text{spin}}$. To ensure a smooth crossover between the two paths, R_3C_3 and R_0C_0 are designed to match.

B. Capacitively Coupled First Stage

The use of a capacitively coupled first stage [30] has three advantages: it has a better power efficiency than current feedback instrumentation amplifiers or three-opamp instrumentation amplifiers; its capacitively coupled input can handle a wide common-mode input range, so that the biasing current of the Hall sensors can be adjusted freely, and a differential sensing structure can be easily implemented by connecting another set of input capacitors to the virtual ground, as shown in Fig. 9. A set of high-ohmic resistors in the feedback define the dc biasing point of the virtual ground. This effectively

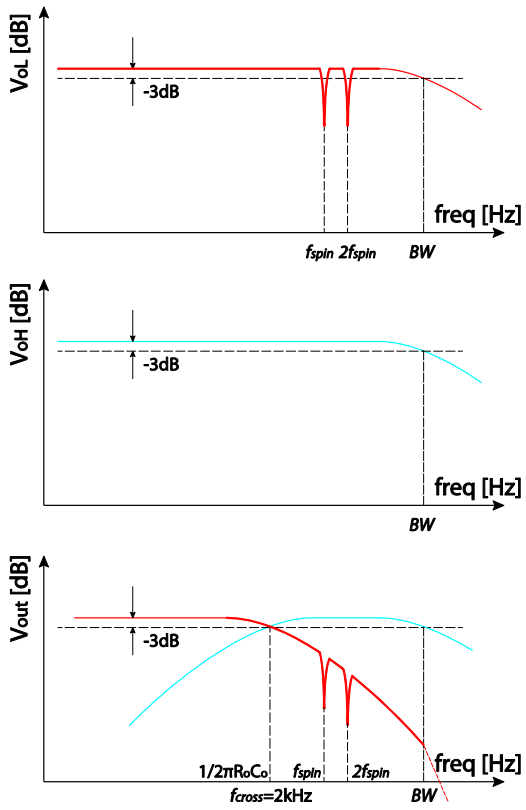

Fig. 8. Bode plots of the LF path, the HF path, and the multipath Hall sensor system.

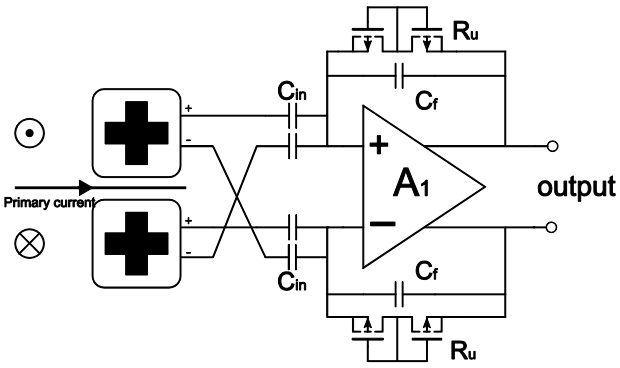

Fig. 9. Capacitively coupled first-stage combines two Hall sensors at the virtual ground to realize a differential measurement.

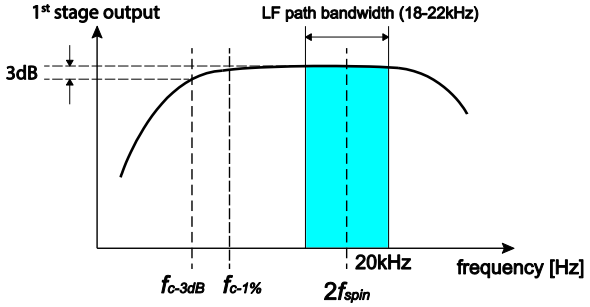

Fig. 10. First stage needs to have a flat bandwidth covering 18–22 kHz.

creates a high-pass filter and configures the opamp in unity gain for offset, which highly relaxes the dynamic range of succeeding stages.

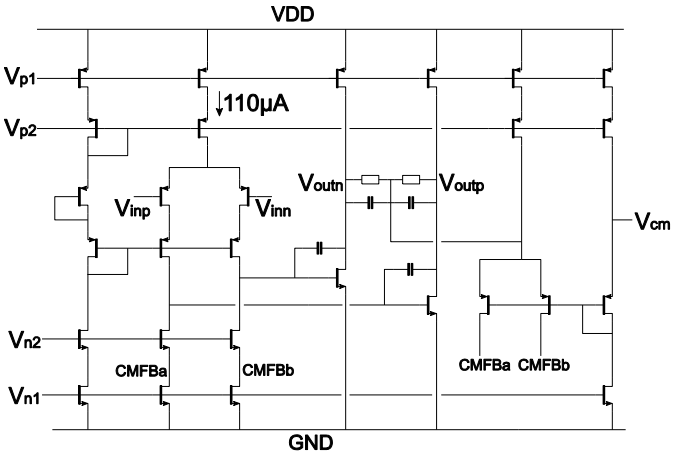

Fig. 11. Implementation of the first opamp A1.

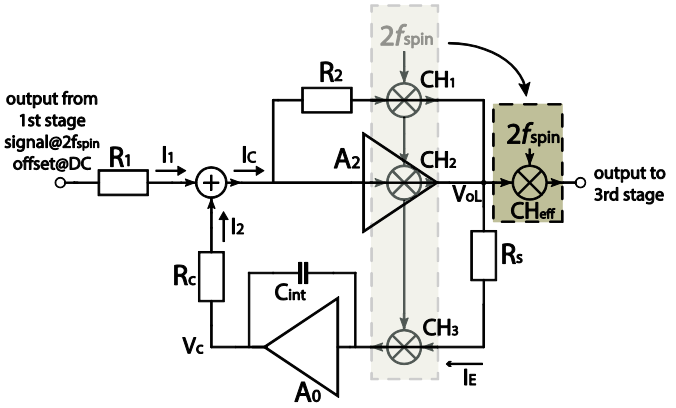

Fig. 12. Implementation model of a single RRL.

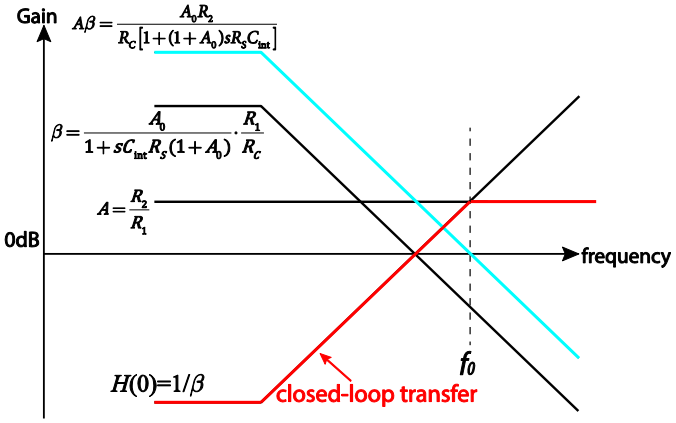

Fig. 13. Bode plot of simplified RRL model.

At the final output, the LF path only contributes signals ranging from dc to 2 kHz. With $f_{\text{spin}} = 10$ kHz, the first stage requires a flat frequency response from 18 to 22 kHz, as shown in Fig. 10. To assure the maximum signal attenuation of $<1\%$ due to the high-pass filtering action, the feedback resistors need to be greater than 370 MΩ ($C_f = 240$ fF). This is achieved by using a pseudoresistor with two back-to-back connected pMOS transistors [31], which results in a resistance of several gigaohms.

Since most of the Hall sensor's offset will be blocked by the input capacitors, the first stage only needs to process the

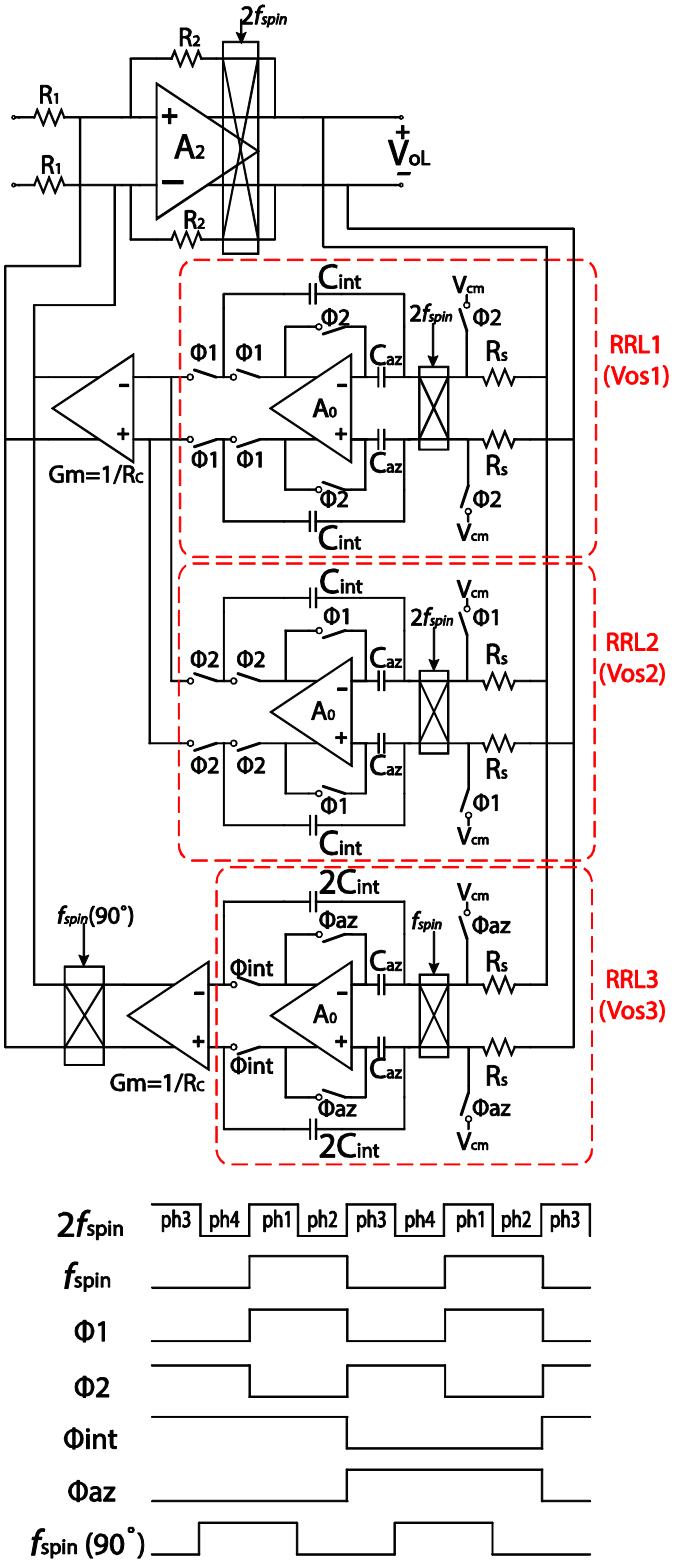

Fig. 14. Complete implementation of the triple RRLs.

magnetic signal and the offset of the first opamp A_1 (~mV). Therefore, A_1 is implemented as a telescopic amplifier with a class-A output to drive the load ($R_1 = 50$ kΩ) of the next stage, as shown in Fig. 11. To achieve a g_m of 1.2 mS, which is commensurate with the sensor's resistance, the input

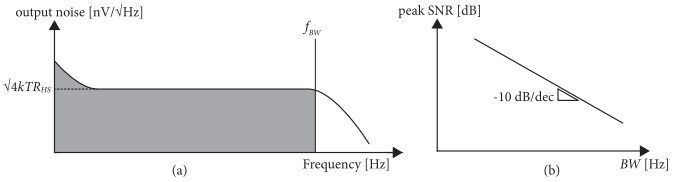

Fig. 15. (a) Output noise of a Hall sensor. (b) Decreasing peak SNR with a slope of −10 dB/decade.

differential pair is biased at 110 μA (out of a total supply current of 175 μA).

C. Implementation of Triple RRLs

Primarily due to the n-well's anisotropic resistance, the Hall sensor's offset changes in different spinning phases. Together with the offset of the first and second stages, it appears as a square-wave ripple at the output of the second stage, which cannot be fully filtered by the output stage. Therefore, triple RRLs are integrated to continuously measure different ripple components (Fig. 6) and inject a compensation signal at the virtual ground of the second stage; 2 out of 3 RRLs are working in a ping (the first and second phases)—pong (the third and fourth phases) sequence to fully compensate any ripple at $2f_{\text{spin}}$. The residual ripple at f_{spin} will be compensated by the third RRL.

In this paper, the RRL implementation is adapted and modified from that in [30], as shown in Fig. 12. Through the sensing resistor R_s, the specific spinning ripple component is converted into current ripple, which is then synchronously demodulated and integrated on a capacitor C_{int}. The compensation is done by injecting a current into the virtual ground of A_2 via R_c. For the sake of parameter analysis, chopper CH_1, CH_2, and CH_3 can be combined to CH_{eff}. This effectively converts the RRL into an active dc servo loop. Assuming A_2 is ideal, then V_{oL} can be expressed as

$$V_{\text{oL}} = (I_1 - I_2)R_2. \tag{2}$$

In the feedback path, the transfer function from V_{oL} to V_{C} can be expressed as

$$\frac{V_C}{V_{\text{oL}}} = \frac{A_0}{1 + (1 + A_0)sR_SC_{\text{int}}} \tag{3}$$

with which (2) can be rewritten as

$$\left[\frac{V_{\text{in}}}{R_1} - \frac{A_0V_{\text{oL}}}{[1 + (1 + A_0)sR_SC_{\text{int}}] \cdot R_C}\right] \cdot R_2 = V_{\text{oL}}. \tag{4}$$

Therefore, the transfer function $H(s)$ from V_{in} to V_{oL} can be expressed as

$$H(s) = \frac{V_{\text{oL}}}{V_{\text{in}}} = \frac{\frac{R_2}{R_1}}{1 + \frac{A_0R_2}{R_C[1+(1+A_0)sR_SC_{\text{int}}]}}. \tag{5}$$

Equation (5) can be mapped into the classical feedback theory, whose corresponding Bode plot is shown in Fig. 13. The loop gain $A\beta$ can be expressed as

$$A\beta = \frac{A_0R_2}{R_C[1 + (1 + A_0)sR_SC_{\text{int}}]} \tag{6}$$

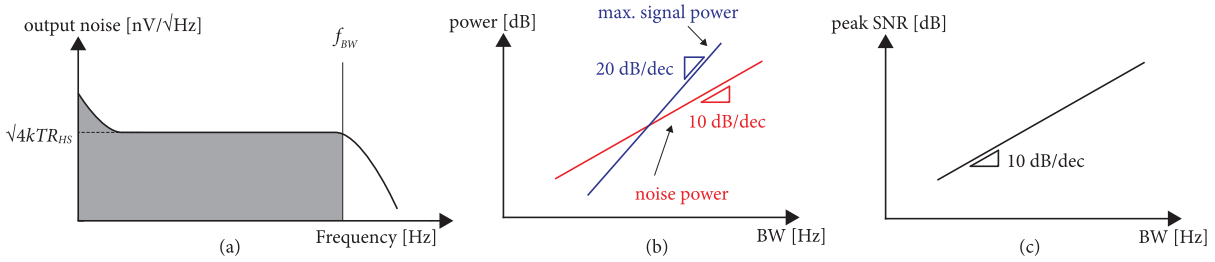

Fig. 16. (a) Output noise of a pickup coil. (b) Increasing noise power with a slope of 10 dB/decade and the increasing signal power with a slope of 20 dB/decade. (c) Decreasing peak SNR with a slope of −10 dB/decade.

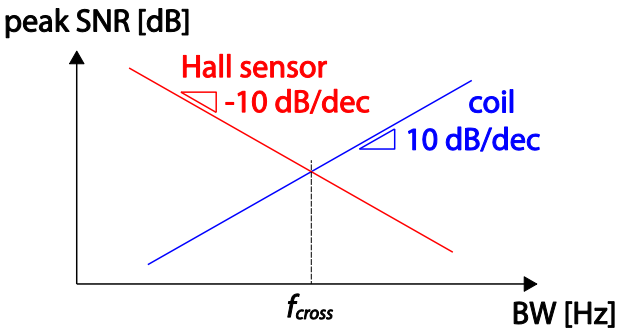

Fig. 17. Peak SNR plots of Hall sensors and coils.

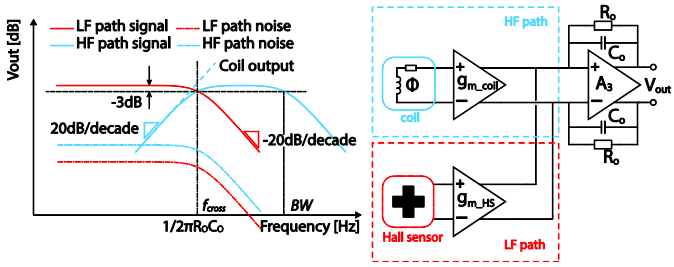

Fig. 18. Proposed network to combine Hall sensors and pickup coils.

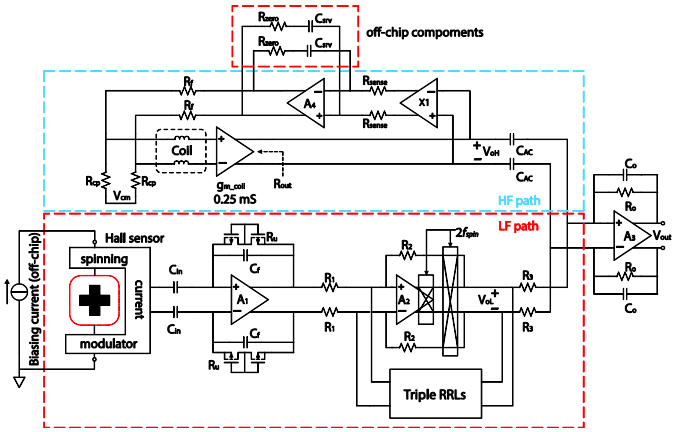

Fig. 19. Detailed implementation of combination of Hall sensors and pickup coils.

with which the high-pass corner frequency f_0 can be calculated as

$$f_0|_{A\beta=1} = \frac{R_2}{2\pi C_{\text{int}} R_S R_C}. \tag{7}$$

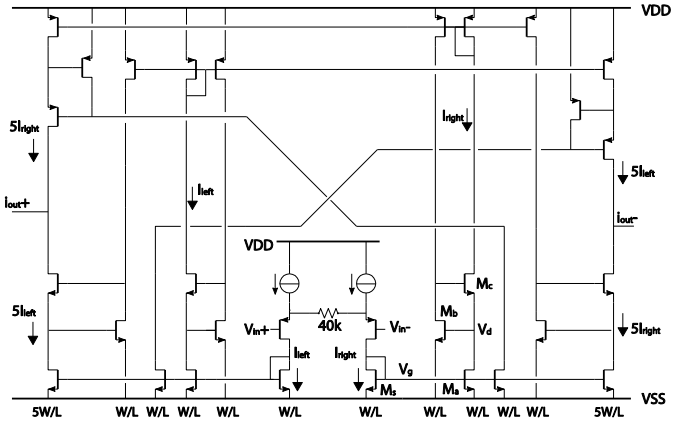

Fig. 20. Implementation of g_{m_coil}.

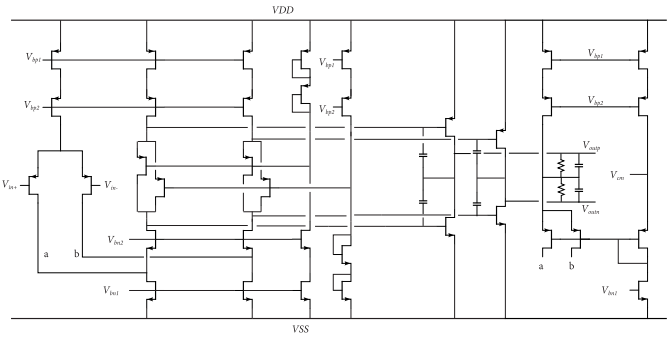

Fig. 21. Implementation of the output stage.

And the dc transfer function can be expressed as

$$H(0) = \frac{R_C}{A_0 \cdot R_1}. \tag{8}$$

The action of chopper CH_{eff} will translate this high-pass filter into a notch filter around the chopping frequency. In this design, $R_1 = 50\,\text{k}\Omega$, $R_2 = 1\,\text{M}\Omega$, $R_S = 10\,\text{M}\Omega$, $C_{\text{int}} = 20\,\text{pF}$, $R_C = 2.5\,\text{M}\Omega$, and $A_0 = 100$ dB, which results in 66 dB of ripple reduction, and a notch width of $2f_0 = 640$ Hz.

The complete implementation of the triple RRLs [28] is shown in Fig. 14. As the residual ripple will be essentially limited by the offset of A_0, all three integrators are autozeroed by storing their offsets on capacitor C_{AZ}. The RRL1 and RRL2 are arranged in a ping-pong sequence: in $\Phi 1$, RRL1 extracts the ripple associated with the first

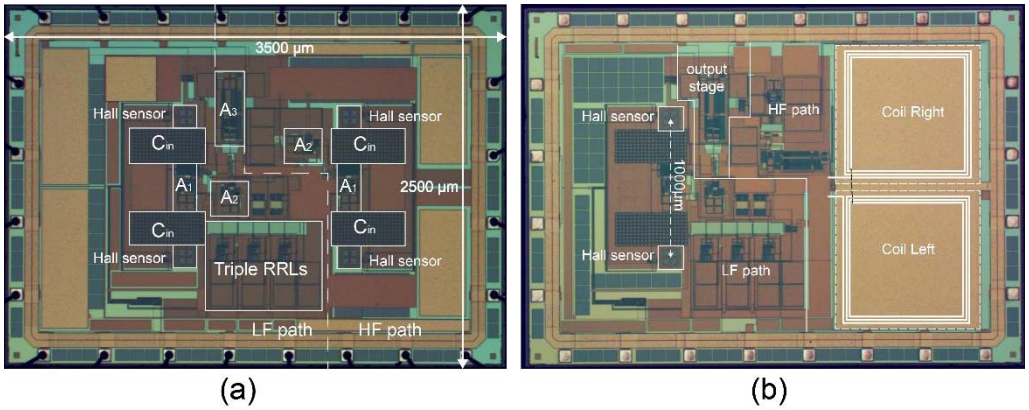

Fig. 22. (a) Chip photo of the multipath Hall sensor system. (b) Chip photo of the system combining Hall sensors and pickup coils.

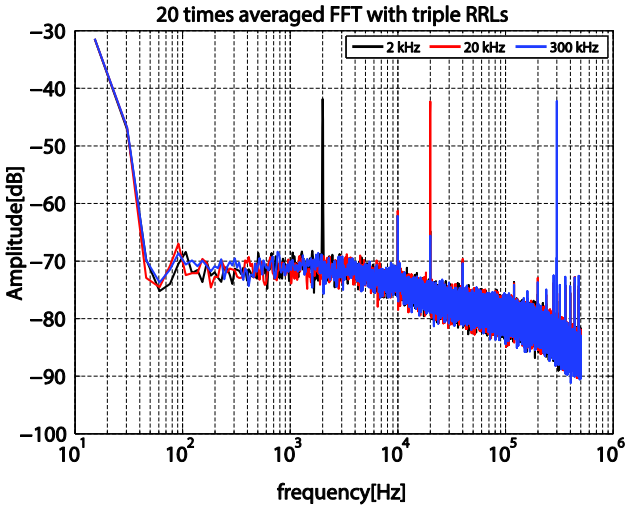

Fig. 23. FFT of the multipath Hall sensor system with input signals at 2, 20, and 300 kHz.

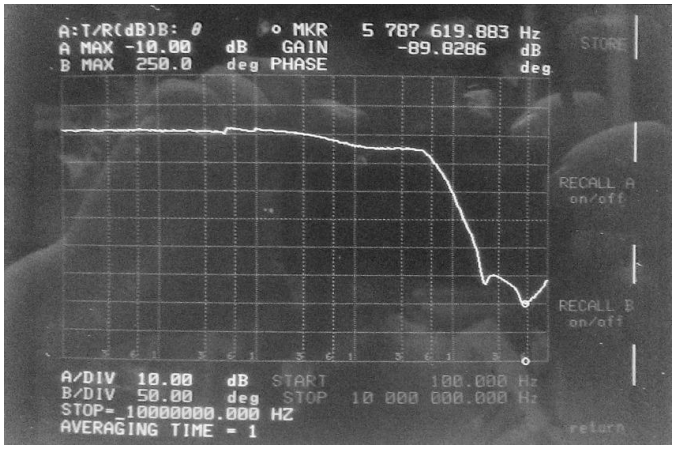

Fig. 24. Bandwidth measurement results of the multipath Hall sensor system, whose HF response is distorted by the eddy current within the frame pad.

and second phases, while RRL2 is in autozeroing mode, and in Φ2, RRL1 is autozeroed, while the ripple associated with the third and fourth phases are extracted by RRL2. The residual ripple is extracted and compensated by RRL3, which is autozeroed once every spinning cycle.

III. Hybrid Multipath System Combining Hall Sensors and Pickup Coils

A. Combination of Hall Sensors and Pickup Coils

Although wide bandwidth and low offset can be simultaneously achieved by the multipath Hall sensor system, its thermal noise power increases linearly with bandwidth, as shown in Fig. 15. For a given bandwidth f_{BW}, the SNR of a Hall sensor can be expressed as

$$\mathrm{SNR}_{\mathrm{HS}} = \frac{(B_{\mathrm{in}} \cdot S_{\mathrm{HS}})^2}{4kT R_{\mathrm{HS}} \cdot f_{\mathrm{BW}}} \tag{9}$$

where R_{HS} and S_{HS} represent the resistance and the sensitivity of the Hall sensor, respectively, and B_{in} represents the magnetic field signal.

Conversely, doubling the bandwidth of a pickup coil will also double its noise power, but quadruple its peak signal power, as shown in Fig. 16. This suggests that the peak SNR of a pickup coil will increase by 3 dB for every doubling of the bandwidth (10 dB/decade). The SNR of a pickup coil in a given bandwidth f_{BW} can be expressed as

$$\mathrm{SNR}_{\mathrm{coil}} = \frac{B_{\mathrm{in}}^2 \cdot (nA)^2 \cdot 4\pi^2 \cdot f_{\mathrm{BW}}^2}{4kT R_{\mathrm{coil}} \cdot f_{\mathrm{BW}}} \tag{10}$$

where n and A represent the number and area of the coil windings, respectively, and R_{coil} represent the resistance of the pickup coil.

As shown in Fig. 17, the peak SNRs of the Hall sensors and the pickup coils will intersect at a certain frequency. At this so-called crossover frequency f_{cross}, the system should maximize SNR by switching from one sensor to another. For a given Hall sensor and a pickup coil, f_{cross} can be calculated as

$$f_{\mathrm{cross}} = \frac{S_{\mathrm{HS}}}{2\pi nA}\sqrt{\frac{R_{\mathrm{coil}}}{R_{\mathrm{HS}}}}. \tag{11}$$

For a Hall sensor with $S_{\mathrm{HS}} = 100$ mV/T and $R_{\mathrm{HS}} = 2$ kΩ and a pickup coil with $n = 32$, $A \approx 1$ mm^2, $R_{\mathrm{coil}} = 20$ kΩ, and $f_{\mathrm{cross}} = 1.5$ kHz. In this design, f_{cross} was intentionally set to 2 kHz in order to leave some margin for readout noise and to save chip area.

Fig. 18 shows the proposed combination network to ensure smooth frequency transition. The Hall sensor in the LF path

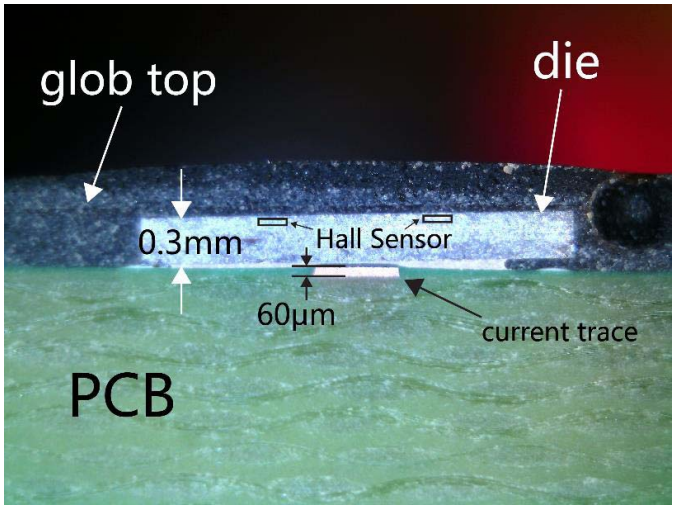

Fig. 25. Cross section of COB sample.

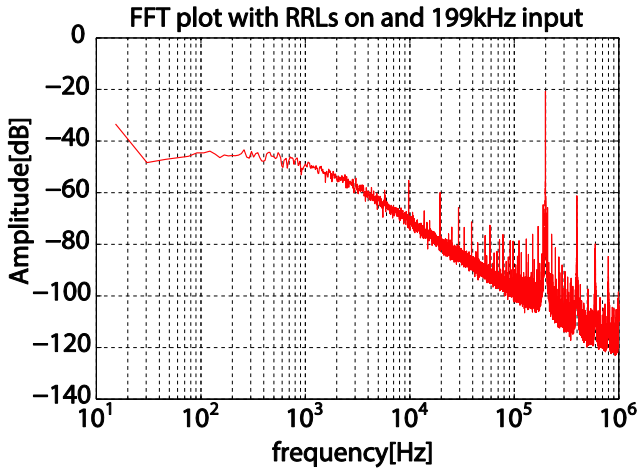

Fig. 26. FFT plot of the hybrid multipath system with an input current at 199 kHz.

and the pickup coil in the HF path are read out by g_{m_HS} and g_{m_coil}, respectively, and then combined by a transimpedance amplifier with a time constant of R_0C_0. The low-pass filtering action of the transimpedance amplifier also limits the noise bandwidth of both Hall sensors and coils, so that wide bandwidth and high resolution can be both achieved. Since only one time constant is involved, the proposed combination network ensures that the crossover frequency is the same for both paths. Spread in the values of R_0 and C_0 will only result in a gain mismatch between the LF and HF paths. This mismatch can be trimmed by adjusting the biasing currents of the Hall sensors.

Due to the presence of the first-order frequency transition, the bandwidth of the LF path needs to be considerably higher than f_{cross} to prevent any overall gain reduction around LF path bandwidth. For instance, to ensure a gain flatness of 0.1 dB (1%), the LF path bandwidth needs to be 100 times larger than f_{cross}, namely, 200 kHz.

B. System Implementation

The implementation of the complete system is shown in Fig. 19. The LF path employs spinning current Hall sensors

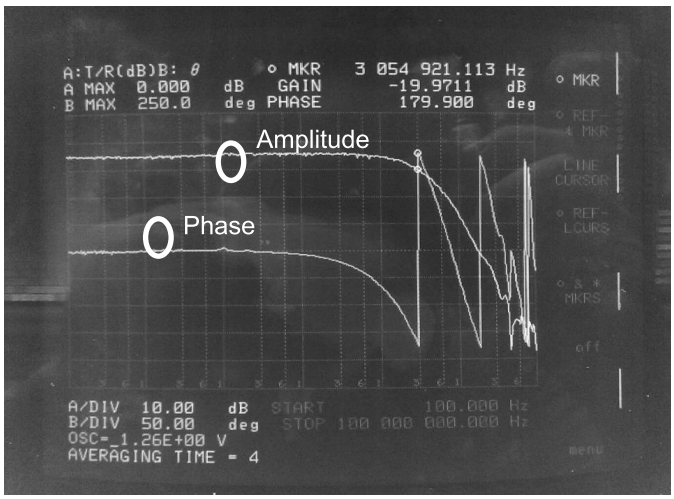

Fig. 27. Measurement result of the amplitude and phase response of the multipath hybrid system over the frequency range from 100 Hz to 100 MHz.

and triple RRLs to ensure low offset, and employs enough bandwidth to ensure a flat frequency response. The implementation is exactly the same as the LF path in the multipath Hall sensor system.

To suppress the offset of g_{m_coil}, coupling capacitors C_{ac} are used to block the dc current. Together with the output impedance R_{out} of g_{m_coil}, C_{ac} effectively creates a high-pass filter whose cut-off frequency is given by $1/2\pi\, R_{\mathrm{out}}C_{\mathrm{ac}}$. Similar to the LF path bandwidth requirement, this corner frequency needs to be 100 times less than f_{cross}, i.e., 20 Hz, to ensure a bandwidth flatness within 0.1 dB. With $C_{\mathrm{ac}} = 20$ pF, R_{out} needs to be larger than 400 MΩ. The circuit diagram of g_{m_coil} is shown in Fig. 20. The input differential pair is degenerated by a 40-kΩ resistor to a maximum linear input range. To maximize the output impedance of the current mirrors, transistors M_a and M_c are cascaded. Moreover, a gain boosting transistor M_b is used to regulate the node V_d to further boost the output impedance of the current mirrors. Instead of biased by a constant current, M_b is biased by a copy of the signal current, so that V_d will be made exactly equal to V_g (the gate potential of transistor M_s). As transistors M_s and M_a are identically biased (gate, source, and drain), the current signal can be accurately mirrored independent of the load, which realizes a large output impedance [32]. For better power efficiency, the differential output currents are also mirrored via pMOS current source to a push–pull output stage. A mirror ratio of 5 results in an effective transconductance of 0.25 mS. With a supply current of 1.35 mA, g_{m_coil} can produce a differential output current of ±250 μA at 5 MHz.

To prevent V_{oH} from clipping, a dc servo loop is built. To preserve the output impedance, V_{oH} is first buffered by a pair of source followers, then converted into current via resistor R_{sense} (5 MΩ) and integrated in C_{srv} (10 μF). Since the loop gain has two poles $R_{\mathrm{sense}}C_{\mathrm{srv}}/A_4$ and $R_{\mathrm{out}}C_{\mathrm{ac}}$, a compensating zero is created by inserting R_{zero} (2 kΩ) in series with C_{srv} to cancel the effect of the nondominant pole $R_{\mathrm{out}}C_{\mathrm{ac}}$.

To accurately handle the large output current from g_{m_coil} at high frequencies, i.e., ±100 μA at 2 MHz, and maximize the

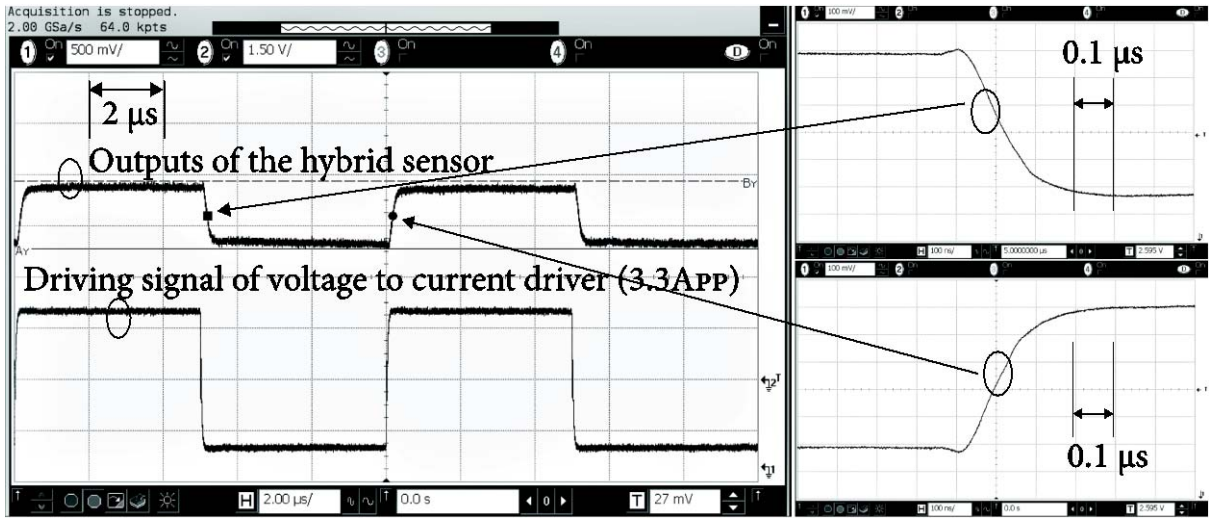

Fig. 28. Step response of the hybrid multipath system, a settling (90%) time of <400 ns has been achieved.

output range, a class-AB output stage with a quiescent current of 940 μA was used. Its circuit diagram is shown in Fig. 21.

IV. Experiment Results

The two proposed systems were fabricated in the same batch of a 0.18-μm CMOS process. The chip photos are shown in Fig. 22. Both chips occupy a total area of 8.75 mm^2. In both designs, each Hall sensor consists of four orthogonally coupled Hall plates, and each Hall plate is covered by a p+ layer to reduce $1/f$ noise by isolating the Si/SiO_2 interface. When biased with a total current of 1.4 mA (0.35 mA for each plate), the Hall sensor has a sensitivity of 50 mV/T, resulting in a combined sensitivity of 100 mV/T. The multipath Hall sensor system consumes a total of 8 mA, 5.6 mA of which is used to bias the four Hall sensors. In the multipath hybrid system, the biasing current of the Hall sensors is adjusted to 2 mA (0.5 mA for each plate), so that the Hall sensors have a sensitivity of 71.4 mV/T (142.8-mV/T combined sensitivity) to match that of the pickup coils. The multipath hybrid system consumes 7.7 mA, 4 mA of which is used to bias the two Hall sensors in the LF path. Measurement on total ten samples of both chips shows a maximum offset of <40 μT. The multipath Hall sensor system can measure a differential field up to 12.5 mT, while the multipath hybrid can measure up to 7.8 mT, with a maximum magnetic field slew rate of 136 mT/μs.

A. Measurement Results of Multipath Hall Sensor Systems

The multipath Hall sensor chip is packed in a ceramic SOIC package to bring down the distance between the current conducing trace and the Hall sensors. This results in a current-to-magnetic transfer of $\sim$0.2 mT/A. With a 1-A primary current, fast Fourier transforms (FFTs) of the sensor's output at 2, 20, and 300 kHz are shown in Fig. 23. It can be noticed that the residual ripple at f_{spin} (10 kHz) is reduced to about -60 dB, equivalent to 7.3 μT, which can be as large as 1.1 mT without triple RRLs. The total integrated noise corresponds to a differential magnetic field resolution of 272 μT_{rms}, or a single-ended resolution of 136 μT_{rms}, which is dominated by the noise of the Hall sensors and the capacitively coupled first stages. Moreover, hardly any harmonic distortion can be seen.

The measured bandwidth of the multipath Hall sensor system is shown in Fig. 24. It extends up to 400 kHz, without any notches, but suffers from a reduction in gain at frequencies above 50 kHz. This is caused by eddy currents induced in the lead-frame pad to which the die is glued. At high frequencies, these currents become large enough to significantly counterbalance the external magnetic field.

B. Measurement Result of the Hybrid Multipath System

To prevent eddy current from distorting the HF response, the hybrid multipath chip is glued directly on top of a PCB trace using the chip-on-board (COB) technique, with the added advantage of close distance between the primary current and sensors. The resulting current-to-magnetic transfer is then increased to about 0.43 mT/A. The cross section of a sample is shown in Fig. 25.

Fig. 26 shows the FFT plot of the hybrid system with a primary current at 199 kHz. Clearly, the noise bandwidth is limited by the output stage to 2 kHz. The noise floor is dominated by the noise from the source resistance of the pickup coil (20 kΩ) as well as g_{m_coil}, which is degenerated by a 40-kΩ resistor. The total integrated noise corresponds to a differential magnetic field resolution of 210 μT_{rms} or a single-ended resolution of 105 μT_{rms}, which can be further improved by reducing the resistance of the pickup coil as well as the noise of g_{m_coil}. The residual ripple at f_{spin} (10 kHz) is about 8 μT, which is similar to that of the multipath Hall sensor system. However, due to the limited linearity of g_{m_coil}, a second-harmonic distortion about -40 dB is present.

Fig. 27 shows the amplitude and phase response of the hybrid multipath system with the biasing current of Hall sensor properly adjusted. A flat frequency response (both amplitude and phase) is achieved with a -3 dB bandwidth of 3 MHz. At higher frequencies (>1 MHz), the phase response rolls off

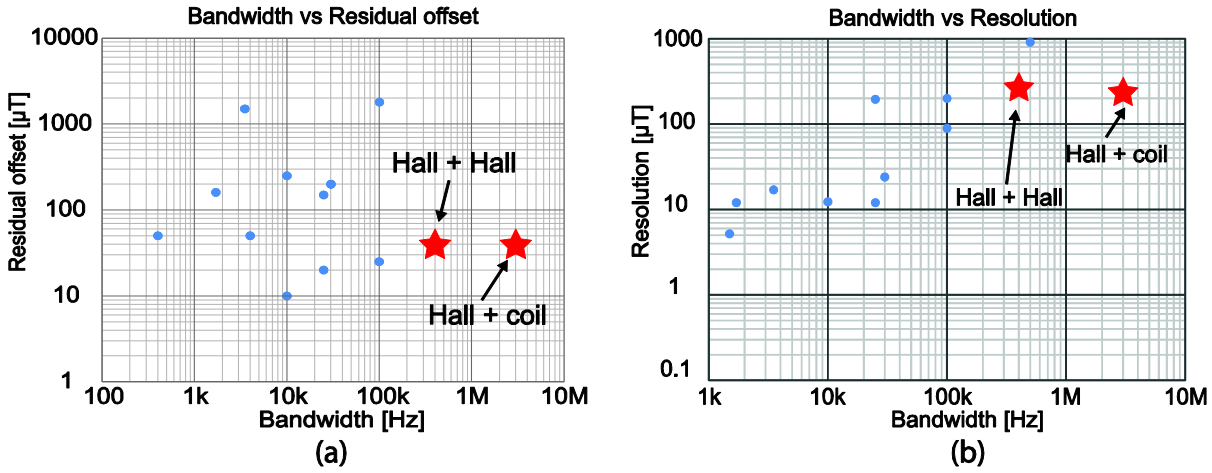

Fig. 29. Benchmark plot of (a) bandwidth versus offset and (b) bandwidth versus resolution.

TABLE I
COMPARISON TABLE

Source	This work		[3]	[14]	[6]	[8]
Sensor type	Hall + coil	Hall + Hall	Fluxgate	Hall	Hall	Hall
Technology	0.18 μm	0.18 μm	0.6 μm	0.35 μm	0.5 μm	0.35 μm
Maximum offset [μT]	40	40	0.9	10	3.65 (3σ)	10
Area [mm^2]	8.75 (analog front-end)	8.75 (analog front-end)	9.8	5.7	N/A	6.5
Resolution [μT_{rms}]	210 (diff)	272 (diff)	0.1	0.6	0.33	N/A
Input range	±7.8 mT (diff)	±12.5 mT (diff)	±1.32 mT (diff)	±0.5 mT	±10.8 mT	N/A
Bandwidth	3 MHz	400 kHz	75 kHz	100 Hz	5 Hz	10 kHz
Output	Analog	Analog	Digital	Digital	Digital	Digital
Supply current [mA]	7.7	8	56	5	4.2	N/A

in a second-order fashion. The bandwidth of the system can also be demonstrated by examining its step response, as shown in Fig. 28. The test was done with a 3.3-A_{pp} square-wave primary current at 100 kHz. The settling of both the rising and falling edges is quite symmetrical, with a settling (>90%) time of <400 ns.

Fig. 29 shows two benchmark plots of bandwidth versus offset and bandwidth versus resolution. It can be seen that the combination of the multipath architecture together with triple RRLs and the spinning current technique breaks the bandwidth-offset tradeoff. Furthermore, the bandwidth-resolution tradeoff has also been broken by exploiting the differentiating characteristic of the pickup coils.

Table I compares the proposed designs against other CMOS magnetic sensors. They are the fastest ever reported with an offset of less than 50 μT. Compared with [8], both achieve comparable offset, but with 40 and 300 times bandwidth improvement, respectively. Although [6] achieves a much better offset, its bandwidth is severely limited by the use of eight-phase spinning and low-pass filtering. The recently introduced fluxgate-based sensor [4] has even better offset. However, despite its higher power consumption, its bandwidth is limited to 75 kHz. The current consumption of the multipath Hall sensor system is somewhat higher than other CMOS Hall sensors due to the extra biasing currents consumed by the Hall sensors in the HF path. Thanks to the differentiating

characteristic of the pickup coils, the extra bandwidth of the hybrid multipath system does not involve a similar tradeoff with power.

V. Conclusion

This paper has proposed a multipath technique for wide-bandwidth CMOS magnetic sensor. Compared with previous low-offset CMOS magnetic sensors, the combination of spinning Hall sensors and nonspun Hall sensors achieves a bandwidth of 400 kHz, a 40 times improvement. The combination of spinning Hall sensors and pickup coils achieves a bandwidth of 3MHz, which represents a further order of magnitude improvement. These two examples demonstrate that the use of multipath architectures effectively breaks the usual design tradeoff between sensor bandwidth, on the one hand, and sensor offset and resolution, on the other.

Acknowledgment

The authors would like to thank Texas Instruments for chip fabrication.

References

[1] S. H. Shalmany, D. Draxelmayr, and K. A. A. Makinwa, "A micropower battery current sensor with ±0.03% (3σ) inaccuracy from −40 to +85°C," in *IEEE ISSCC Dig. Tech. Papers*, Feb. 2013, pp. 386–387.

[2] C. Xiao, L. Zhao, T. Asada, W. G. Odendaal, and J. D. van Wyk, "An overview of integratable current sensor technologies," in *Proc. 38th IAS Annu. Meeting Conf. Rec. Ind. Appl. Conf.*, vol. 2. Oct. 2003, pp. 1251–1258.

[3] F. Rothan, C. Condemine, B. Delaet, O. Redon, and A. Giraud, "A low power 16-channel fully integrated GMR-based current sensor," in *Proc. Conf. ESSCIRC*, Sep. 2012, pp. 245–248.

[4] M. Kashmiri, W. Kindt, F. Witte, R. Kearey, and D. Carbonell, "A 200kS/s 13.5b integrated-fluxgate differential-magnetic-to-digital converter with an oversampling compensation loop for contactless current sensing," in *IEEE ISSCC Dig. Tech. Papers*, Feb. 2015, pp. 490–491.

[5] M. F. Snoeij, V. Schaffer, S. Udayashankar, and M. V. Ivanov, "An integrated fluxgate magnetometer for use in closed-loop/open-loop isolated current sensing," in *Proc. 41st ESSCIRC/ESSDERC Conf.*, Sep. 2015, pp. 263–266.

[6] J. C. van der Meer, F. R. Riedijk, E. van Kampen, K. A. Makinwa, and J. H. Huijsing, "A fully integrated CMOS Hall sensor with a 3.65μT 3σ offset for compass applications," in *IEEE ISSCC Dig. Tech. Papers*, Feb. 2005, pp. 246–247.

[7] P. Kejik, P. F. Bourdelle, S. Reymond, F. Salvi, and P. A. Farine, "Offset compensation based on distributed Hall cell architecture," *IEEE Trans. Magn.*, vol. 49, no. 1, pp. 105–108, Jan. 2013.

[8] M. Motz *et al.*, "A miniature digital current sensor with differential Hall probes using enhanced chopping techniques and mechanical stress compensation," in *Proc. IEEE Sensors*, Oct. 2012, pp. 1–4.

[9] M. Nymand and M. A. Andersen, "High-efficiency isolated boost DC–DC converter for high-power low-voltage fuel-cell applications," *IEEE Trans. Ind. Electron.*, vol. 57, no. 2, pp. 505–514, Feb. 2010.

[10] S.-W. Hong *et al.*, "High area-efficient DC-DC converter with high reliability using time-mode Miller compensation (TMMC)," *IEEE J. Solid-State Circuits*, vol. 48, no. 10, pp. 2457–2468, Oct. 2013.

[11] B. Miedzinski, A. Szymanski, W. Dzierzanowski, and B. Wojszczyk, "Performance of Hall sensors when used in ground fault protections in MV networks," in *Proc. 39th Int. Univ. Power Eng. Conf. (UPEC)*, Sep. 2004, pp. 753–757.

[12] A. Elez, S. Car, and Z. Maljkovic, "Detection of inter-coil short circuits in synchronous machine armature winding on the basis of analysis of machine magnetic field," in *Proc. 19th Int. Conf. Elect. Mach. (ICEM)*, Sep. 2010, pp. 1–6.

[13] F. Blaabjerg, J. K. Pedersen, U. Jaeger, and P. Thoegersen, "Single current sensor technique in the DC link of three-phase PWM-VS inverters: A review and a novel solution," *IEEE Trans. Ind. Appl.*, vol. 33, no. 5, pp. 1241–1253, Sep. 1997.

[14] C. Schott, R. Racz, A. Manco, and N. Simonne, "CMOS single-chip electronic compass with microcontroller," *IEEE J. Solid-State Circuits*, vol. 42, no. 12, pp. 2923–2933, Dec. 2007.

[15] P. Dimitropoulos, P. M. Drljaca, and R. S. Popovic, "A 0.35μm-CMOS, wide-band, low-noise Hall magnetometer for current sensing applications," in *Proc. IEEE Sensors*, Oct. 2007, pp. 884–887.

[16] R. S. Vanha, "Rotary switch and current monitor by Hall-based microsystems," Phys. Electron. Lab., Swiss Federal Inst. Technol., Zürich, Switzerland, Tech. Rep. 13135, 1999.

[17] K. Skucha, P. Liu, M. Megens, J. Kim, and B. Boser, "A compact Hall-effect sensor array for the detection and imaging of single magnetic beads in biomedical assays," in *Proc. 16th Int. Solid-State Sens. Actuators Microsyst. Conf. (TRANSDUCERS)*, Jun. 2011, pp. 1833–1836.

[18] Y.-J. Min and S.-W. Kim, "A CMOS TDC-based digital magnetic Hall sensor using the self temperature compensation," in *Proc. IEEE Custom Integr. Circuits Conf. (CICC)*, Sep. 2008, pp. 329–332.

[19] Y. Xu, H.-B. Pan, S.-Z. He, and L. Li, "Monolithic H-bridge brushless DC vibration motor driver with a highly sensitive Hall sensor in 0.18 μm complementary metal-oxide semiconductor technology," *IET Circuits Devices Syst.*, vol. 7, no. 4, pp. 204–210, Jul. 2013.

[20] Z. B. Randjelovic, M. Kayal, R. Popovic, and H. Blanchard, "Highly sensitive Hall magnetic sensor microsystem in CMOS technology," *IEEE J. Solid-State Circuits*, vol. 37, no. 2, pp. 151–159, Feb. 2002.

[21] S. Brugger and O. Paul, "Magnetic field amplification by slender cuboid-shaped magnetic concentrators with a single gap," *Sens. Actuators A, Phys.*, vol. 157, no. 1, pp. 135–139, 2010.

[22] C. Schott, R. Racz, and S. Huber, "Smart CMOS sensors with integrated magnetic concentrators," in *Proc. IEEE Sensors*, Nov. 2005, pp. 959–962.

[23] P. J. A. Munter, "A low-offset spinning-current Hall plate," *Sens. Actuators A, Phys.*, vol. 22, nos. 1–3, pp. 743–746, Jun. 1990.

[24] L. M. Stephenson and H. E. M. Barlow, "Power measurement at 4 Gc/s by the application of the Hall effect in a semiconductor," *Proc. IEE B, Radio Electron. Eng.*, vol. 106, no. 25, pp. 27–30, Jan. 1959.

[25] R. Wu, J. H. Huijsing, and K. A. Makinwa, "A current-feedback instrumentation amplifier with a gain error reduction loop and 0.06% untrimmed gain error," *IEEE J. Solid-State Circuits*, vol. 46, no. 12, pp. 2794–2806, Dec. 2011.

[26] M. Motz, D. Draxelmayr, T. Werth, and B. Forster, "A chopped Hall sensor with small jitter and programmable 'true power-on' function," *IEEE J. Solid-State Circuits*, vol. 40, no. 7, pp. 1533–1540, Jul. 2005.

[27] J. Jiang, W. J. Kindt, and K. A. A. Makinwa, "A continuous-time ripple reduction technique for spinning-current Hall sensors," *IEEE J. Solid-State Circuits*, vol. 49, no. 7, pp. 1525–1534, Jul. 2014.

[28] J. Jiang and K. A. A. Makinwa, "A multi-path CMOS Hall sensor with integrated ripple reduction loops," in *Dig. ASSCC*, Nov. 2015, pp. 53–56.

[29] J. Jiang and K. Makinwa, "A hybrid multipath CMOS magnetic sensor with 210$\mu\mathrm{T_{rms}}$ resolution and 3MHz bandwidth for contactless current sensing," in *IEEE ISSCC Dig. Tech. Papers*, Feb. 2016, pp. 204–205.

[30] Q. Fan, F. Sebastiano, J. H. Huijsing, and K. A. A. Makinwa, "A 1.8 μW 60 nV/$\sqrt{\text{Hz}}$ capacitively-coupled chopper instrumentation amplifier in 65 nm CMOS for wireless sensor nodes," *IEEE J. Solid-State Circuits*, vol. 46, no. 7, pp. 1534–1543, Jul. 2011.

[31] R. R. Harrison and C. Charles, "A low-power low-noise CMOS amplifier for neural recording applications," *IEEE J. Solid-State Circuits*, vol. 38, no. 6, pp. 958–965, Jun. 2003.

[32] A. Zeki and H. Kuntman, "High-output-impedance CMOS dual-output OTA suitable for wide-range continuous time filtering applications," *Electron. Lett.*, vol. 35, no. 16, pp. 1295–1296, Aug. 1999.

Junfeng Jiang received the B.Sc. degree from the Dalian University of Technology, Dalian, China, in 2009, and the M.Sc. degree from the Delft University of Technology, Delft, The Netherlands, in 2011, where he is currently pursuing the Ph.D. degree with the Electronic Instrumentation Laboratory, with a focus on the design of a wide-bandwidth contact-less current sensor.

He is also with Texas Instruments, Dallas, TX, USA, as an Analog Designer.

Kofi A. A. Makinwa (M'97–SM'05–F'11) received the B.Sc. and M.Sc. degrees from Obafemi Awolowo University, Ife, Nigeria, in 1985 and 1988, respectively, the M.E.E. degree from the Philips International Institute, Eindhoven, The Netherlands, in 1989, and the Ph.D. degree from the Delft University of Technology, Delft, The Netherlands, in 2004.

From 1989 to 1999, he was a Research Scientist with Philips Research Laboratories, Eindhoven, where he was involved in interactive displays and on front ends for optical and magnetic recording systems. He joined the Delft University of Technology in 1999, where he is currently an Antoni van Leeuwenhoek Professor. He holds 25 patents. He has authored ten books and over 200 technical papers. His current research interests include the design of precision mixed-signal circuits, sigma-delta modulators, smart sensors, and sensor interfaces.

Dr. Makinwa is an elected member of the IEEE Solid-State Circuits Society AdCom and the society's governing board. He received the 2005 Simon Stevin Gezel Award from the Dutch Technology Foundation. He was a co-recipient of several best paper awards from the JOURNAL OF SOLID-STATE CIRCUITS (JSSC), International Solid-State Circuits Conference (ISSCC), Transducers, and European Solid-State Circuits Conference (ESSCIRC) among others. He is an alumnus of the Young Academy of the Royal Netherlands Academy of Arts and Sciences. He is on the program committees of the ISSCC, the VLSI Symposium, the ESSCIRC, and the Advances in Analog Circuit Design workshop. He has also served as a Guest Editor of the JSSC and as a Distinguished Lecturer of the IEEE Solid-State Circuits Society.